Ultra-stiff, strong, and highly thermally conductive crystalline graphitic films with mixed stacking order

Bin Wang,[1] Benjamin V. Cunning,*[1] Na Yeon Kim,[1, 3] Fariborz Karger[4], Sun-Young Park,[1, 3] Zhancheng Li,[5] Shalik R. Joshi,[6] Li Peng,[7] Vijayakumar Modepalli,[1] Xianjue Chen,[1] Yongtao Shen,[1] Won Kyung Seong,[1] Youngwoo Kwon,[1] Jeongsu Jang,[8] Haofei Shi,[5] Chao Gao,[7] Gun-Ho Kim,[6] Tae Joo Shin,[9] Kwanpyo Kim,[8] Ju-Young Kim,[1, 3] Alexander A. Balandin[4], Zonghoon Lee,[1, 3] Rodney S. Ruoff*[1, 2, 3]

[1] Center for Multidimensional Carbon Materials (CMCM), Institute for Basic Science (IBS), Ulsan 44919, Republic of Korea.

[2] Department of Chemistry, Ulsan National Institute of Science and Technology (UNIST), Ulsan 44919, Republic of Korea.

[3] School of Materials Science and Engineering, Ulsan National Institute of Science and Technology (UNIST), Ulsan 44919, Republic of Korea.

[4] Phonon Optimized Engineered Materials (POEM) Center, Department of Electrical and Computer Engineering, University of California, Riverside, California 92521 USA.

[5] Chongqing Institute of Green and Intelligent Technology, Chinese Academy of Sciences, Chongqing 400714, P. R. China.

[6] Department of Mechanical Engineering, Ulsan National Institute of Science and Technology (UNIST), Ulsan 44919, Republic of Korea.

[7] MOE Key Laboratory of Macromolecular Synthesis and Functionalization, Department of Polymer Science and Engineering, Key Laboratory of Adsorption and Separation Materials & Technologies of Zhejiang Province, Zhejiang University, 38 Zheda Road, Hangzhou 310027, P. R. China.

[8] Department of Physics, Ulsan National Institute of Science and Technology (UNIST), Ulsan 44919, Republic of Korea.

[9] UNIST Central Research Facilities & School of Natural Science, Ulsan National Institute of Science and Technology (UNIST), Ulsan 44919, Republic of Korea.

*Correspondence to: ben.cunning@gmail.com, rsruoff@ibs.re.kr, ruofflab@gmail.com

Abstract:

We report a macroscopic (~2.5 cm × 2.5 cm) crystalline graphitic film composed of 100 stacked graphene layers made by layer-by-layer assembly of 100 chemical vapor deposited single layer graphene films, that has significantly higher stiffness and fracture strength than other macroscale films made of solely graphene or graphite, along with a high in-plane electrical conductivity and thermal conductivity. The graphene layers were transferred and stacked one by one using a wet process that led to layer defects and interstitial contamination. Heat treatment of the sample up to 2800 °C resulted in the removal of interstitial contaminants and the healing of graphene layer defects. The resulting stacked graphene sample is a freestanding film with long-range order in the *(002)* direction. We found that the graphene layers have near perfect in-plane crystallinity but a mixed stacking order (turbostratic/AB co-exist) through the thickness, which separates it from all existing carbon materials including natural graphite, turbostratic carbon, or CVD-grown multilayer graphene samples. Macroscale tensile tests yielded values of Young's modulus of 62 GPa and a fracture strength of 0.70 GPa, higher than has been reported for any other macroscale carbon films made of only graphene or graphite with no other constituents. Micro-scale tensile tests yielded even higher performance,

a maximum Young's modulus of 290 GPa and fracture strength of 5.8 GPa when stretching parallel to the film. In-plane measurements of electrical and thermal conductivity revealed exceptional values of 2.2 $\times 10^5$ S m^{-1} and 2292±159 W m^{-1} K^{-1} respectively. The high performance of these films is attributed to the combination of the high in-plane crystalline order and unique stacking configuration through the thickness.

Graphene could be an excellent building block for mechanically strong films given its *intrinsic* Young's modulus (1.1 TPa) and tensile strength (~130 GPa).[1,2] However, the intrinsic strength has been found only at the micron-length scale. We recently used a new method to measure the mechanical strength of multi-centimeter single layer graphene grown by chemical vapor deposition (CVD); the average strength of those macroscale samples was 4.5 GPa, and the average Young's modulus was 793 GPa.[3] To date, macroscale samples made of only stacked and overlapped graphene platelets (no other constituents) had Young's moduli lower than 50 GPa and fracture strengths of around 100 MPa.[4-9] These significantly lower values are likely due to a combination of factors; graphene flakes being synthesized with defects, imperfect and irregular stacking of graphene flakes due in part to their random lateral sizes and shapes, and film preparation techniques that result in voids.[10]

As CVD graphene continues to improve due to efforts worldwide to grow "higher and higher" quality material, it is sensible to ask what types of macroscale samples can be made with many layers that have been individually stacked and what will their properties be? We

have attempted to provide a preliminary answer to this question by creating samples with many centimeter-scale graphene layers stacked one by one, here totaling 100, as this is the thinnest film that can be suspended over a centimeter-scale hole in our experiments.

Stacking of 2D materials is a promising approach to create van der Waals structures,[11-14] but until recently, these structures have been limited by the small size of the exfoliated 2D crystals and it is difficult to envision the established techniques being useful for a large number of stacked layers -such as 100 large area graphene layers. Layer-by-layer assembly of CVD-grown wafer-scale transition-metal dichalcogenide (TMD) films on SiO_2/Si substrates by a vacuum dry transfer method was reported,[15] however, this method cannot be used in stacking large area monolayer CVD-graphene films grown on Cu foils as it has not been possible (to date) to get defect-free large graphene layers by direct peeling.[16] Large-scale CVD-grown graphene films are usually transferred and stacked by a wet process using a polymer as a support material.[17] This transfer process typically introduces defects within each graphene layer such as cracks and voids, as well as significant residues on the surface of the graphene.[18] As a result, assembling these wet-transferred graphene layers into a stacked structure is likely to result in a defective material due to defects in plane and interstitial contamination between layers. The defects are detrimental for optimal electrical as well as mechanical and thermal properties.[19,20]

Here, we have made centimeter-scale crystalline films by stacking 100 layers of CVD-grown graphene, with the resulting film demonstrating significantly higher stiffness, fracture strength, and thermal conductivity than any other macroscale film composed of only graphene or graphite without other constituents. The freestanding film sample resulting from layer-by-layer stacking was subjected to successive annealing treatments of 400 °C (**SG400**), 2000 °C (**SG2000**), and 2800 °C (**SG2800**) in Ar for two hours at each temperature (see time-temperature profile in **Fig. S1**), and the evolution from stacked but discrete layers of graphene to a new macroscale synthetic material was studied. The interstitial contaminants introduced during the stacking process were 'driven out' by heating to 2800 °C while layer defects were also repaired. The resulting stacked graphene sample is a freestanding film with no contaminants between the graphene layers. Given the polycrystalline graphene used, a stacked structure should be almost entirely turbostratic. However, we have found that high temperature annealing 'drove' the formation of some regions towards AB-stacking that resulted in mixed turbostratic/AB-stacking throughout the sample. This unique stacking order differentiates the sample from existing carbon materials (including graphite, glassy carbon, and grown multilayer graphene). The Young's modulus, fracture strength and in-plane thermal conductivity are higher than any other reported macro-scale carbon film materials made of solely graphene or graphite. These results suggest the potential for applications of such 'layer-by-layer assembled' CVD grown graphene layers.

Because poly(methyl methacrylate) (PMMA) always leaves a residue on the graphene surface during its removal,[18] a stacking process that has a single PMMA support layer on only the top layer of graphene was used, to minimize the amount of residue between each graphene layer. Our approach for stacking 100 layers of graphene is shown schematically in **Fig. 1a.** First, a PMMA support layer was coated onto a monolayer of polycrystalline graphene grown on a Cu foil. The copper was etched in an iron chloride ($FeCl_3$) solution and the sample transferred to water to attempt to remove any residue from the etching process. The floating PMMA/graphene was then lifted out of the water by a second graphene/Cu foil resulting in a PMMA/graphene/graphene/copper stack. This "etching process followed by lift-out" was repeated until a stack of 100 graphene layers was obtained. The PMMA layer at the top was dissolved in acetone and the remaining assembly was heated to 400 °C in Ar/H_2 to obtain the stacked graphene (**SG400**) sample. To heat the sample to higher temperatures, the **SG400** film was transferred onto a hollow graphite plate such that the **SG400** film spanned the orifice. Heating the sample on a solid substrate would cause the film to stick and could not be separated for further study. We found it was not possible to realize the transfer by the widely used 'polymer-assisted' wet transfer method as the high surface tension of the liquid (water or acetone) broke the film in the regions it was not supported by the substrate. Our recently discovered 'camphor-enabled' transfer method was instead used to transfer the film from Cu foil to the hollow graphite plate successfully as shown in Fig. 1a.[3] A solid camphor layer was first deposited on the **SG400** film on a Cu foil as a support, and the Cu was etched away. After transferring the camphor/**SG400** onto the

hollow graphite plate, the camphor was sublimated in air and then the sample was successively heated to 2000 °C (**SG2000**) and then 2800 °C (**SG2800**). More details are in the **Methods** in the **Supporting Information**. The resulting **SG2800** is a free-standing thin film about 2.5 cm × 2.5 cm in area and composed of 100 well-stacked graphene layers with a total sample thickness of ~35 nm as shown in: (i) the scanning electron microscopy (SEM) image (Fig. 1b, inset is the photo of the **SG2800** film on a hollow graphite plate), (ii) an atomic force microscopy (AFM) image and the corresponding height profile (Fig. 1c), and (iii) a cross-sectional transmission electron microscopy (TEM) image (Fig. 1d). Wrinkles were observed on the film as shown in the SEM and AFM images and the photo in Fig. 1b, which are observed after heating at 2000 °C on the hollow graphite template and possibly caused by the shrinkage of the film during heating in a suspended state. The surface roughness of the film is 21.0 nm RMS as measured by AFM (**Table S1**).

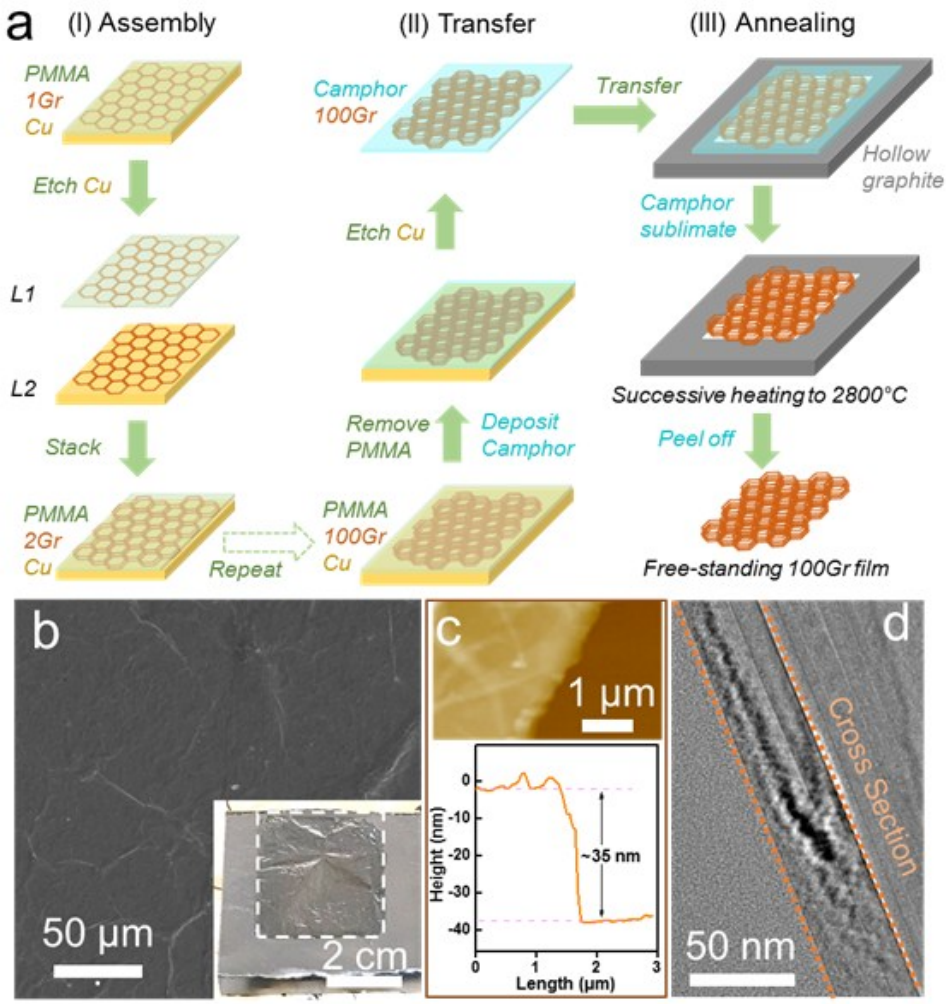

Fig. 1. (a) Schematic of the preparation of the stacked graphene film sample including assembly, transfer, and annealing. (b) An SEM image obtained from the surface of the stacked 100 layers of graphene after heating at 2800 °C (**SG2800**), and a photo showing the free-standing thin film on a hollow graphite plate (inset). The AFM (c) and cross sectional TEM (d) images showing the film with a thickness of around 35 nm supported on a Si substrate (right) with a sputtered carbon protecting layer (left).

To investigate the structural variation of the stacked graphene film by annealing from 400 °C to 2800 °C, we first characterized the **SG400** sample by cross-sectional TEM with energy dispersive X-ray spectroscopy (EDX) and electron energy loss spectroscopy (EELS), Raman spectroscopy, synchrotron grazing incidence wide-angle X-ray scattering (GIWAXS), and powder X-ray diffraction (XRD).

A TEM cross-section of the stack is shown in **Fig. 2** a-d, and further in **Fig. S2**. At a low resolution in both bright field (Fig. 2a) and high angle annular dark field (HAADF) images (**Fig. S3**a), large variations of contrast were apparent due to the presence of both voids and metallic nanoparticles throughout the film. A high magnification image of a region containing a void is shown in Fig. 2b. The metallic particles were characterized by EDX in scanning transmission electron microscopy (STEM) mode (Fig. 2d), and GIWAXS (Fig. 2g-h, and **S4a**) revealing them to be a mixture of Cu and Fe, arising from metal salts trapped between the layers that originated from the reaction between the growth substrate (forming $CuCl_2$) and the etching solution ($FeCl_3$). The low temperature annealing of these metal salts in a reducing environment surrounded by carbon resulted in the detection of the metal, rather than the salt in the X-Ray analysis. Carbon K-edge EELS spectra (Fig. S3c) taken at most points also showed the sample has a mixture of graphitic and amorphous regions. The amorphous carbon signature is likely from 'adventitious carbon' in the atmosphere that rapidly adsorbs on the graphene

surface after its removal from the CVD reactor.[21,22] Regions with well stacked layers were examined using high-resolution TEM (HRTEM) and images are shown in Figs. 2c and **S5**, which show an average d-spacing between the layers of 3.50 ± 0.11 Å, larger than the value of 3.355 Å from graphite,[23] suggesting turbostratic stacking between the graphene layers.[24] GIWAXS and powder XRD measurements (**Figs. S6** and **S7**) also show a broad *(002)* peak located at 1.85 $Å^{-1}$ (q, GIWAXS) and 25.92° (2-Theta, XRD), corresponding to d-spacing values of 3.42 Å and 3.44 Å respectively (**Table 1**), similar to turbostratic carbon (3.43 Å).[24]

Table1: Measured interlayer spacing of graphene layers in each sample by XRD methods (laboratory diffraction instrument, synchrotron source).

Sample	XRD d-spacing (Å)	GIWAXS d-spacing (Å)	*(002)* FWHM (2θ)[a]	L_c (nm)[b]
SG400	3.44	3.42	1.54	5.24
SG2000	3.41	3.42	0.97	8.3
SG2800	3.36	3.39	0.46	18
HOPG (SP-1)	3.36	3.37	0.24	34

a: FWHM values are reported from the laboratory XRD data. b: L_c values are calculated using the Scherrer equation from the *(002)* FWHM.

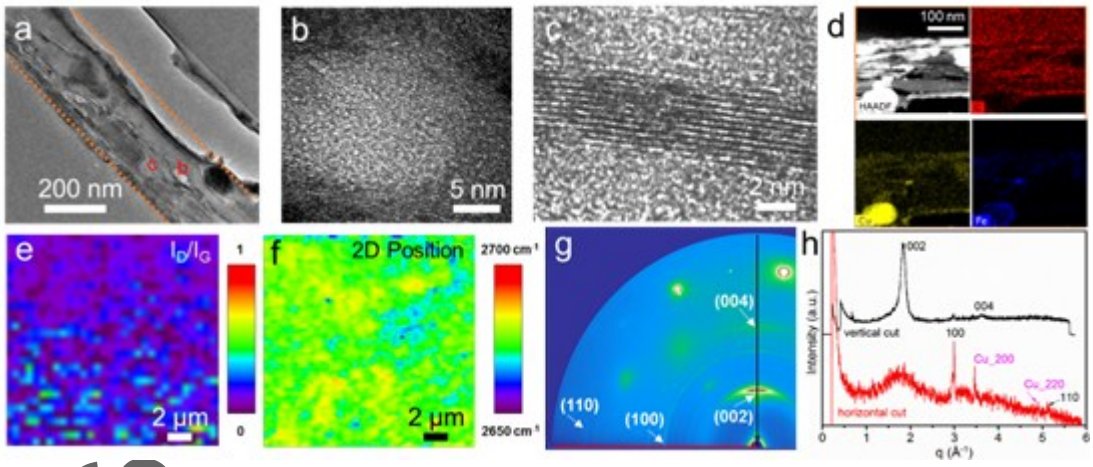

Fig. 2. Characterization of the stacked graphene sample treated at 400 °C (**SG400**). (a) Cross-sectional bright field TEM image, with labeled regions further magnified showing a void (b) and the layered graphene structure (c). (d) High angle annular dark field (HAADF) image and energy dispersive X-ray images in scanning transmission electron microscopy mode (STEM EDX elemental maps) showing the presence of C, Cu and Fe in the film. (e) Raman maps of the intensity ratio of D band to G band (I_D/I_G,) and (f) peak position of the 2D band for **SG400**. (g) Grazing incidence wide-angle X-ray scattering (GIWAXS) 2D pattern of **SG400** on a sapphire substrate. (h) 1D X-Ray scattering patterns from the vertical and horizontal line cuts indicated on the 2D GIWAXS pattern.

The Raman spectrum (**Fig. S8**) and map of the intensity ratio of the D to G bands (I_D/I_G) (Fig. 2e) show that basal plane defects are present in **SG400**, generated during the transfer and stacking process since no D band was observed on the pristine monolayer graphene as-grown on Cu foils. A map of the 2D band peak position is shown in (Fig. 2f and **S9**) and displays an

average position of 2674 cm^{-1}, which is typical for single layer graphene[25] and ~20 cm^{-1} lower than the value typical for turbostratic stacked graphene layers.[26] The **SG400** sample consists of very weakly interacting graphene layers due to both interstitial contamination and the turbostratic stacking (as a result of the micron sized grains of each graphene layer stacking with a random orientation with respect to the directly adjacent layers) results in a 2D peak position closer to that of single layer graphene rather than turbostratic graphite.

From our analysis it is clear that the pristine stacked graphene sample obtained by wet transfer and stacking contain a significant number of defects and contamination from interstitial adventitious carbon and metal nanoparticles. In an attempt to remove the interstitial contamination and basal plane defects we subjected the **SG400** film to further annealing. First, **SG400** was annealed in Ar at 2000 °C for 2 hours (**SG2000**). **SG2000** was then annealed (thus, a second time) at 2800 °C for two hours (**SG2800**).

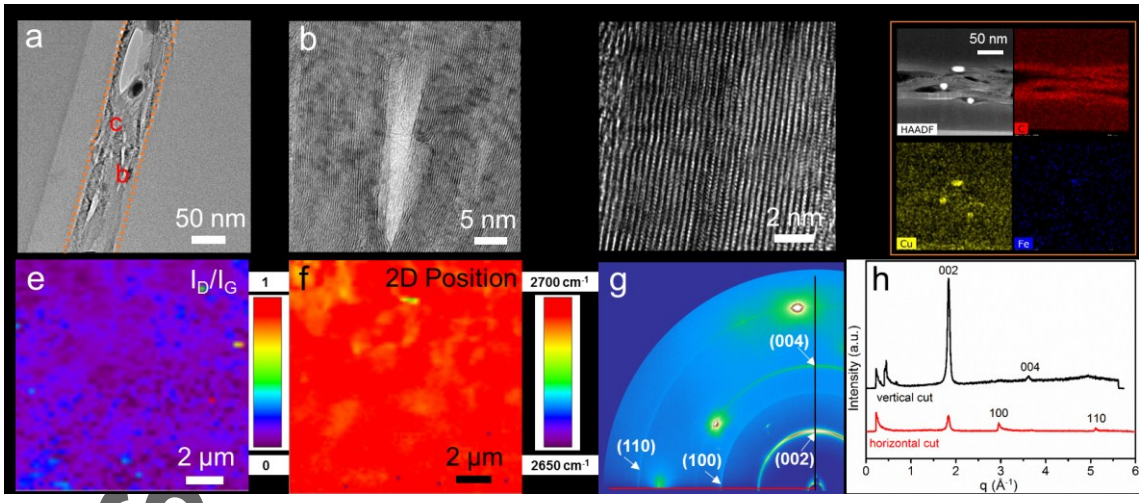

Fig. 3. Characterization of the sample heated at 2000 °C in Ar for 2 hours (**SG2000**). (a) Cross-sectional TEM image, with labeled regions further magnified showing (b) a void and (c) a region with graphitic layer structure. (d) HAADF and STEM-EDX elemental maps indicating that C and Cu are present in the film. Raman maps of (e) the intensity ratio of D to G bands (I_D/I_G) and (f) the peak position of the 2D band for **SG2000**. (g) GIWAXS scattering 2D pattern of **SG2000** on a sapphire substrate. (h) 1D X-Ray scattering patterns from the vertical and horizontal line cuts indicated on the 2D GIWAXS pattern.

The TEM cross-section images of **SG2000** (**Fig. 3**a-d and **S10**) show that voids and metal particles are present in lower concentrations than in the **SG400** sample. The graphene layers are seen to be spatially diverging in many regions near to the regions of contamination. In contrast to the **SG400** sample, the graphene layers can be seen more clearly in the TEM image and exist over thicker regions indicating that the annealing has improved interfacial contact between the layers; we attribute this to the removal of significant amounts of interstitial

adventitious carbon. This is confirmed by the sharp discrete carbon K-edge in EELS (**Fig. S11**) as it displays a much more graphitic signature for the stacked graphene layers in **SG2000** as compared to **SG400**. XRD analysis (Fig. S7) and HRTEM images (**Fig. S12**) show the average interlayer spacing decreased to 3.41 Å and 3.39±0.11 Å, respectively. Further analysis of GIWAXS (Fig. 3g-h and **S13**) data on **SG2000** revealed clear diffraction from the *(002)* as well as the *(004)* planes suggesting long range 00*l* order, as well as the presence of in-plane 'graphite' *(100)* and *(110)* planes that were absent from the **SG400** sample. The angular broadening of the *(100)* and *(110)* planes in the 2D GIWAXS image shows that there is a large range of (local) layer-to-layer orientations in the sample. Regions in the TEM cross-section images show voids and 'spatially diverging' stacked graphene layers, and the latter is the reason for the angular broadening of the *(002)* plane observed in the GIWAXS image. Statistical analysis of the Raman spectra (Figs. 3e-f and S8) revealed that the I_D/I_G ratio is lower than in the **SG400** sample, demonstrating that annealing 'healed' a significant fraction of the defects present in the basal plane. The average peak position of the 2D band in **SG2000** also increased to 2697 cm^{-1} from 2675 cm^{-1} in the **SG400** sample. The high temperature treatment at 2000 °C has shifted the 2D peak position from a value close to single layer graphene to a value observed in turbostratic graphite samples[27] suggesting annealing has increased the interlayer interaction between the stacked layers. This is further confirmed by the analysis of the second-order Raman modes which show features of turbostratic stacking (**Fig S14**).[28,29]

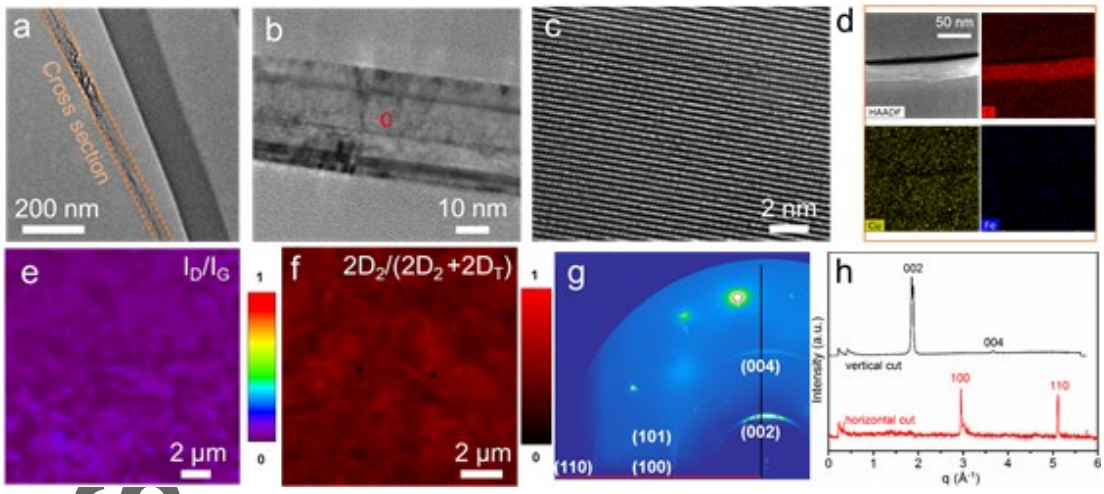

Fig. 4. Characterization of the stacked graphene sample heated at 2800 °C in Ar for 2 hours (**SG2800**). (a) Cross-sectional bright field TEM image, and (b-c) magnified images show the well-stacked graphene layers. (d) HAADF and STEM-EDX elemental maps indicating the film is composed of carbon without Cu and Fe. (e) Raman map of I_D/I_G, (f) Map of the fraction of AB stacking order from the fitted 2D band. (g) Synchrotron GIWAXS scattering 2D pattern of **SG2800** on a sapphire substrate. (h) 1D X-Ray scattering patterns from the vertical and horizontal line cuts indicated on the 2D GIWAXS pattern.

When the **SG2000** sample was heated to 2800 °C for 2 h, TEM cross section images and elemental mapping (**Fig. 4**a-d, and **Fig. S15**) show that the contamination and the voids in the structure were removed, and the graphene layers were now closely stacked and close to parallel throughout the entire cross-section in the checked regions. The carbon EELS spectrum (**Fig. S16**) shows a very graphitic signature similar to that of high-oriented pyrolytic graphite (HOPG)[30] which suggests that the interstitial carbon contamination observed in the samples

heated at lower temperatures had been removed or graphitized. While we cannot conclusively rule out sp^3 formation, none of our analysis suggests that it is present in a quantity that could affect the material properties. The boiling points of Cu and Fe are 2567 °C and 2750 °C respectively, and so metal particles are likely converted to atoms or small clusters that are driven out of the film at 2800 °C, also allowing the graphene layers to more closely stack.

The Raman map in Fig. 4e shows a very low I_D/I_G value, on average less than 0.05, suggesting that structural defects were also repaired for the heating at 2800°C. The 2D band of the Raman spectrum is very sensitive to the stacking configuration of the layers.[31] In turbostratic graphite (incommensurate stacking), the 2D band exists as a single symmetric peak, which splits into an asymmetric peak in hexagonal graphite.[27] With regions of turbostratic and AB stacking order, the fraction of AB stacking order can be estimated by fitting the 2D band with 3 Lorentzian peaks (2 for AB stacked graphite ($2D_1$: ~2680 cm^{-1}, and $2D_2$: ~2720 cm^{-1}) and one for turbostratic graphite ($2D_T$: 2700 cm^{-1}) (**Fig. S17**).[27] The degree of AB stacking at each Raman data point is then assigned as $2D_2 / (2D_2 + 2D_T)$. Peak areas are used here. From the maps and histogram in Fig. 4f and **S18**, respectively, the fraction of AB stacking in these samples is thereby found to be in the range of 0.3~0.5. From this analysis it is clear that the 2800°C annealing caused some regions in the sample to undergo a rearrangement to form AB stacking. In regions of the sample which contained a large fraction of AB stacking as indicated by 2D band deconvolution, we observed a strong 'oTO' band

(~1750 cm^{-1}, the out-of-plane transverse optical phonon) and suppressed 'iTALO' band (~1860 cm^{-1}, combination of the in-plane transverse acoustic and the longitudinal optical phonons) in the second order region of the spectrum whilst in regions of the sample which were mostly turbostratic, the attenuated 'oTO' band and stronger 'iTALO' band further confirm the turbostratic stacking (see **Fig S14**).[28,29] We also exfoliated the **SG2800** sample using the 'scotch tape' method to prepare samples with a few layers for observing the stacking order between the graphene layers using dark-field TEM analysis (**Fig. S19**).[32-34] Similar to the results of the Raman analysis, some regions displayed turbostratic stacking while other regions displayed AB stacking. While the exact mechanism of this transformation from turbostratic to AB stacking is unclear, it seems unlikely that (only) layer rotation, even if localized in small regions, can occur. There may be other effects occurring. Both iron and copper, well known graphitization catalysts,[35] were detected in samples annealed at 2000 °C, but disappeared at 2800 °C. Their removal may be associated with a catalytic transformation to AB stacking (that is, covalent bond-breaking and bond-making). Also, the rate of self-diffusion of carbon at 2800°C is not insignificant.[36,37] At regions of thermodynamic instability such as overlapping grain-boundaries or basal plane defects, there could be a transformation to an AB stacked structure caused by the self-diffusion of carbon atoms. To compare this behavior with the structural evolution of other types of carbon materials upon heating, we prepared two thin films that were heat treated to 2800 °C under the same conditions as **SG2800**. A graphitizable

thin film polymer (SU-8) which when heated develops graphitic structural units that grow and fuse in stages as the temperature increases,[38,39] and a graphene oxide (G-O) thin film which already possesses graphitic in-plane structure due to it being derived from graphite, but in small micron-sized flakes. The G-O film represents an intermediate structural state between the graphitizable polymer and the **SG2800**, which has an entire graphitic plane developed in each layer. Eight Raman spectra from random regions on each film were averaged and the 2D bands were fitted as shown in **Fig. S20**. The heated SU-8 film shows a 2D feature typical for AB graphite, while the heated G-O shows predominantly AB stacking with a small $2D_T$ peak, indicating that there is a much lower energy barrier for precursors with smaller graphitic units to transform to AB stacking.

X-Ray scattering analysis (Figs. 4g-h, S6-7, and **S21**) of the **SG2800** sample also indicates significantly increased order in the c axis direction as the *(002)* and *(004)* diffraction peaks are narrower than for **SG2000**. This was true of all other observed diffraction peaks indicating that the graphene layers became more ordered. A faint reflection in the 2D pattern from the *(101)* plane also appeared confirming the AB stacking order indicated by Raman spectra in some regions but its low intensity and the lack of higher order (*10l)* peaks suggest the AB stacking regions are randomly distributed throughout the sample and may not persist through many layers. A lower interlayer spacing was observed for **SG2800** with GIWAXS

giving a value of 3.39 Å, while powder XRD and HRTEM gave values of 3.36 and 3.37 ± 0.13 Å, respectively (**Fig. S22**), similar to the value of 3.36 Å for HOPG.

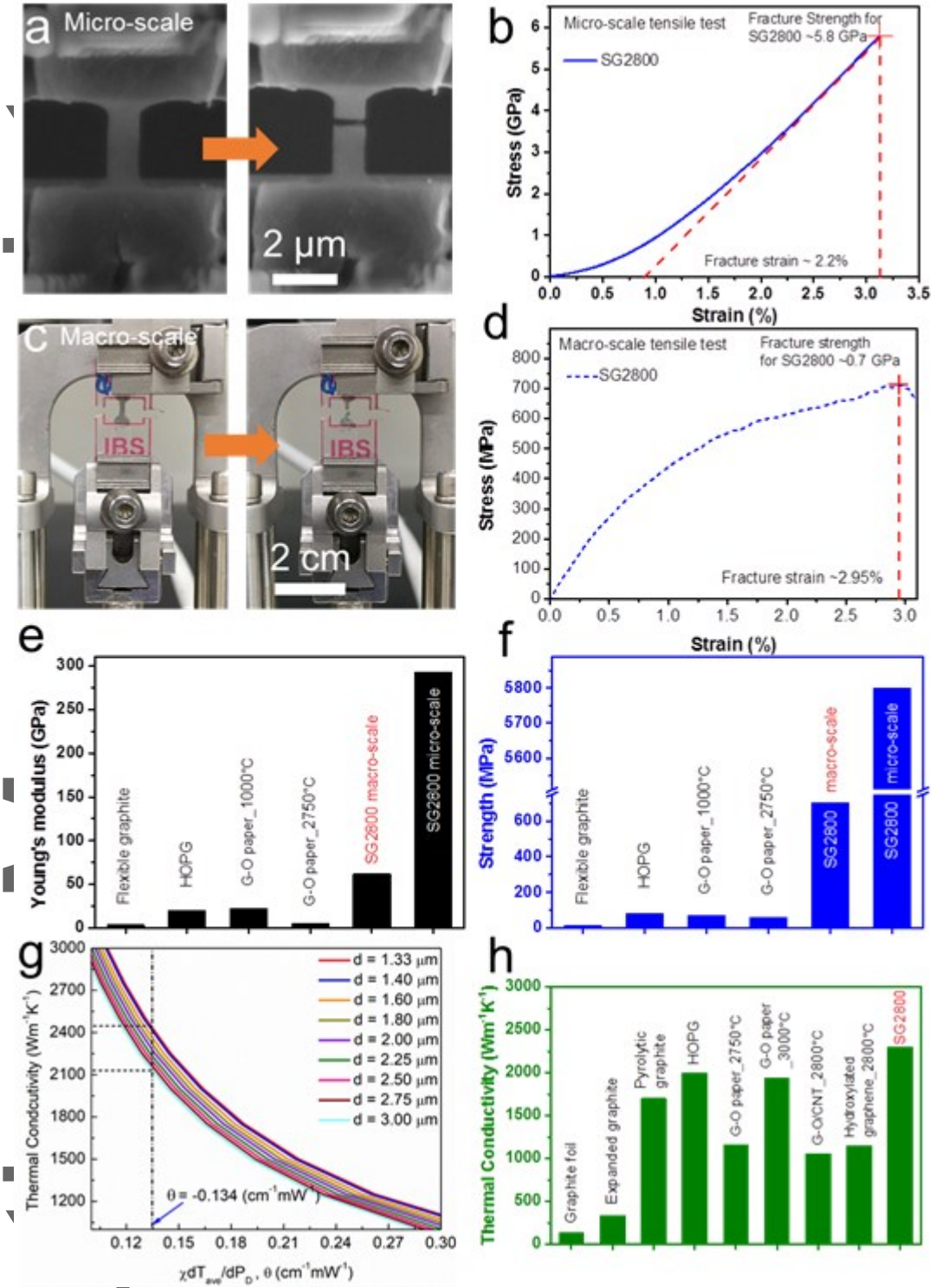

Fig. 5. (a) SEM images showing the micro-scale **SG2800** film under a uniaxial tensile load on a push-to-pull (PTP) device before and after specimen fracture. (b) A typical stress-strain plot for **SG2800** as obtained from the micro-scale tensile test. (c) Images showing the macro-scale polycarbonate film supported **SG2800** film (**PC-SG2800**) under a uniaxial tensile load on a DMA instrument before and after specimen fracture. (d) An extracted stress-strain plot for **SG2800** as obtained from the macro-scale tensile test. (e-f) Comparison of Young's modulus and strength for a set of film materials made of solely graphene or graphite with no other constituents. (g) Numerical simulation results detailing the relationship between sample thermal conductivity and θ using various laser spot sizes. The dot-dashed line highlights θ as measured for **SG2800** and the dashed line indicates the thermal conductivity range based on laser spot size uncertainty. (h) Comparison of thermal conductivity for a set of carbon materials with **SG2800.**

The stress-strain relationship for **SG2800** was first evaluated using in-situ SEM micro-tensile testing as shown in **Fig. 5**a-b and **S23**. Three specimens were examined and the results are shown in **Table S2**. The typical stress-strain curve in Fig. 5b shows brittle fracture of the sample with a fracture strength of 5.8 GPa. It is noted that the initial non-linear region in the stress-strain curve is possibly caused by the non-ideal alignment between the specimen and the as-applied tensile force directions, and also a "straightening" process happening in the beginning of the tensile loading. By measuring the slope of the curve in the linear region, a

Young's modulus of 260 GPa was obtained, and the fracture strain was 2.2%. The average values for Young's modulus, fracture strain and strength from three measured **SG2800** samples are 260±30 GPa, 1.9±0.3%, and 4.8±1.0 GPa, respectively, and the highest values are respectively 290 GPa, 2.2%, and 5.8 GPa; this synthetic crystalline graphitic material thus has a high fracture strength and a high value of Young's modulus, for a film material—at this length scale of a few microns.

A macro-scale tensile test of **SG2800** was also conducted as shown in Fig. 5c-d. Due to the ~35 nm thickness of **SG2800**, the measurement of a freestanding macro-scale film is challenging. A camphor-enabled transfer method for tensile testing of large-scale ultrathin films was recently invented by our group,[3] and it was used to measure the properties of the thin **SG2800** films. A polycarbonate (PC) film with thickness of 240 nm was used as a support and the details are in **Methods**. Three samples with geometry of ~4 mm × 1 mm (length × width) were measured, see **Tables S2-3** and **Fig. S24**. The average values from three measured samples for Young's modulus, fracture strain, and strength for macro-scale **SG2800** are 51.1±9.30 GPa, 1.96±0.90 %, and 0.51±0.17 GPa, respectively, and the highest values are respectively 62 GPa, 3.0 %, and 0.70 GPa. The decreased mechanical performance of the millimeter-scale samples with respect to the micro-scale samples is possibly due to rare regions of discontinuity in the planar direction of the stacked which cause mechanical failure at lower strengths but were avoided in our micro-scale samples. These discontinuous graphene layers

could be generated during transfer (voids generated) and heat treatment processes, and thus are likely a cause of the lower stiffness and strength of the material at macro-scale.[40] A Weibull analysis on the strength of the 3 samples is shown in **Fig. S25**. The Weibull modulus for the micro-scale tested samples is 6.0, and is 2.3 for the macro-scale tested samples. Since the Weibull modulus describes the variability in the measured strength of the materials, and higher values indicates lower variability, the micro-scale samples thus have more uniformly distributed defects/voids than the macro-scale samples, which results in higher strength in the tensile measurements. (A caveat here is that typically ~20 samples are used for Weibull analysis. The challenge of making even 3 samples precluded such a large sample number.)

Although the macro-scale films exhibited lower mechanical performance than the micro-scale films, the tensile modulus and strength are still much higher than those reported for other macro-scale carbon film materials made of solely graphene or graphite with no other constituents, *e.g.* flexible graphite foil prepared by rolling of expanded graphite,[5] HOPG,[4,7,8] 1000 °C reduced graphene-oxide (G-O) paper, and G-O paper first hot-pressed at 2000°C and then annealed at 2750°C for 1 hour (Fig. 5e-f, **Table S4**).[9] We suggest that the enhanced mechanical properties of these films is due to the boundary of each graphene domain (2D grain) *not* overlapping with a domain boundary (i.e., grain boundary) in its adjacent layers, greatly inhibiting failure propagation. This contrasts to graphite materials with 3D grains in that mechanical failure at a grain can cause a cascading effect through the thickness. Moreover,

the large graphene films guarantee the force transfer during stretching and thus a more uniform force distribution as compared with the graphite or graphene flakes composed films, where the discrete nature of the graphene particles inhibits the efficient force transfer and may lead to the local concentration of force and fast failure of the material. The gauge length of the samples used for tensile measurements is summarized in **Table S5**.

Besides stiffness and strength, the sheet resistance for the samples was also evaluated from the current-voltage curves in **Fig. S26**, as 880 Ω/sq (**SG400**), 350 Ω/sq (**SG2000**), and 130 Ω/sq (**SG2800**). For mechanically exfoliated graphene with around 100 layers from HOPG, the reported sheet resistance was ~100 Ω/sq.[41] Considering the thickness of the film of 35 nm, the in-plane electrical conductivity is 2.2 ×10^5 S/m, comparable to HOPG (~10^6 S/m)[42] and rG-O films reduced at 2750 °C (2.2 ×10^5 S/m),[9] and higher than the graphite films made of compacted graphite powder (10^4 ~ 10^5 S/m),[43] G-O films (0.1 S/m),[9] and chemically reduced G-O films (~10^3 S/m).[44] The thermal conductivity of the films was also evaluated by the Raman optothermal technique,[19] using an accurate numerical solution of the heat diffusion equation for the entire sample (**Fig. S27**, see also the **Methods**).[45] From Fig. 5g, the graphene films reveal an exceptionally high thermal conductivity of 2292±159 $Wm^{-1}K^{-1}$ at room temperature by considering the heat transport both on the sample surface and through the film thickness. The measured thermal conductivity is higher than graphite and high-temperature and high pressure treated graphene films, including graphite foil,[9]

expanded graphite,[46] commercial pyrolytic graphite,[47] HOPG,[19] G-O paper pressed and heat treated at 2750°C or 3000°C,[9,48] G-O/CNT composite film or hydroxylated graphene film heat treated at 2800°C [49,50] (Fig. 5h and **Table S6**). The superb in-plane thermal conduction properties have been attributed to the high-quality defect-free individual layers of graphene used in the layer-by-layer assembly of the films. The high thermal conductivity of the films, coupled with their excellent mechanical properties, large lateral dimensions and precisely controlled thickness, open up possibilities for thermal management applications as heat spreaders and thermally conductive coatings.

Our work makes several critical contributions: i) this is the first work to prepare a self-standing macroscopic carbon film made of only large area CVD-graphene materials, and this method can be extended to other 2D materials; ii) this material is a new graphitic structure which has mixed turbostratic and AB stacking modes between highly aligned large graphene layers, resulting in a unique structure that separates it from all existing carbon materials including natural graphite, turbostratic carbon, or CVD-grown multilayer graphene samples; iii) the macroscopic film has significantly higher stiffness, strength, and thermal conductivity than any other macroscale films composed of solely graphene or graphite, and also high electrical conductivity. We have recently achieved CVD growth of large area single crystal graphene and the stacking of such single crystal layers will be the subject of future work. Other groups have also developed CVD methods for growth of single crystals of other

2D materials such as h-BN, MoS_2, $MoSe_2$ (and others) and we believe such stacking approaches could generate significant interest for making "synthetic crystalline films" of other 2D material superlattices that are unobtainable by standard synthesis methods.

References:

1 Lee, C., Wei, X., Kysar, J. W. & Hone, J. Measurement of the Elastic Properties and Intrinsic Strength of Monolayer Graphene. *Science* **321**, 385-388, (2008).

2 Lee, G.-H. *et al.* High-Strength Chemical-Vapor–Deposited Graphene and Grain Boundaries. *Science* **340**, 1073-1076, (2013).

3 Wang, B. *et al.* Camphor-Enabled Transfer and Mechanical Testing of Centimeter-Scale Ultrathin Films. *Adv. Mater.* **30**, 1800888, (2018).

4 Blakslee, O. L., Proctor, D. G., Seldin, E. J., Spence, G. B. & Weng, T. Elastic Constants of Compression-Annealed Pyrolytic Graphite. *J. Appl. Phys.* **41**, 3373-3382, (1970).

5 Dowell, M. B. & Howard, R. A. Tensile and compressive properties of flexible graphite foils. *Carbon* **24**, 311-323, (1986).

6 Dikin, D. A. *et al.* Preparation and characterization of graphene oxide paper. *Nature* **448**, 457-460, (2007).

7 Miyake, S. & Wang, M. Nanoprocessing of layered crystalline materials by atomic force microscopy. *Nanoscale Res. Lett.* **10**, 123, (2015).

8 Meng, X. *et al.* Broad modulus range nanomechanical mapping by magnetic-drive soft probes. *Nat. Commun.* **8**, 1944, (2017).

9 Chen, X. *et al.* Graphitization of graphene oxide films under pressure. *Carbon* **132**, 294-303, (2018).

10 Gong, T. *et al.* Thickness Dependence of the Mechanical Properties of Free-Standing Graphene Oxide Papers. *Adv. Funct. Mater.* **25**, 3756-3763, (2015).

11 Britnell, L. *et al.* Field-Effect Tunneling Transistor Based on Vertical Graphene Heterostructures. *Science* **335**, 947-950, (2012).

12 Geim, A. K. & Grigorieva, I. V. Van der Waals heterostructures. *Nature* **499**, 419-425, (2013).

13 Haigh, S. J. *et al.* Cross-sectional imaging of individual layers and buried interfaces of graphene-based heterostructures and superlattices. *Nat. Mater.* **11**, 764-767, (2012).

14 Liu, Y. *et al.* Van der Waals heterostructures and devices. *Nat. Rev. Mater.* **1**, 16042, (2016).

15 Kang, K. *et al.* Layer-by-layer assembly of two-dimensional materials into wafer-scale heterostructures. *Nature* **550**, 229-233, (2017).

16 Luo, D. *et al.* Role of Graphene in Water-Assisted Oxidation of Copper in Relation to Dry Transfer of Graphene. *Chem. Mater.* **29**, 4546-4556, (2017).

17 Li, X. *et al.* Transfer of Large-Area Graphene Films for High-Performance Transparent Conductive Electrodes. *Nano Lett.* **9**, 4359-4363, (2009).

18 Liang, X. *et al.* Toward Clean and Crackless Transfer of Graphene. *ACS Nano* **5**, 9144-9153, (2011).

19 Balandin, A. A. Thermal Properties of Graphene and Nanostructured Carbon Materials. *Nat. Mater.* **10**, 569-581, (2011).

20 Malekpour, H. *et al.* Thermal Conductivity of Graphene with Defects Induced by Electron Beam Irradiation. *Nanoscale* **8**, 14608-14616, (2016).

21 Li, Z. *et al.* Water Protects Graphitic Surface from Airborne Hydrocarbon Contamination. *ACS Nano* **10**, 349-359, (2016).

22 Li, Z. *et al.* Effect of airborne contaminants on the wettability of supported graphene and graphite. *Nat. Mater.* **12**, 925, (2013).

23 Howe, J. Y., Rawn, C. J., Jones, L. E. & Ow, H. Improved crystallographic data for graphite. *Powder Diffr.* **18**, 150-154, (2012).

24 Franklin, R. E. Crystallite growth in graphitizing and non-graphitizing carbons. *Proceedings of the Royal Society of London. Series A. Mathematical and Physical Sciences* **209**, 196-218 (1951).

25 Wang, Y. y. *et al.* Raman Studies of Monolayer Graphene: The Substrate Effect. *J. Phys. Chem. C* **112**, 10637-10640, (2008).

26 Garlow, J. A. et al. Large-Area Growth of Turbostratic Graphene on Ni(111) via Physical Vapor Deposition. *Sci. Rep.* **6**, 19804, (2016).

27 Cançado, L. G. *et al.* Measuring the degree of stacking order in graphite by Raman spectroscopy. *Carbon* **46**, 272-275, (2008).

28 Rao, R. *et al.* Effects of Layer Stacking on the Combination Raman Modes in Graphene. *ACS Nano* **5**, 1594-1599, (2011).

29 Cong, C. *et al.* Second-Order Overtone and Combination Raman Modes of Graphene Layers in the Range of 1690-2150 cm^{-1}. *ACS Nano* **5**, 1600-1605, (2011).

30 Bernier, N. *et al.* A methodology to optimize the quantification of sp2 carbon fraction from K edge EELS spectra. *J. Electron Spectrosc.* **164**, 34-43, (2008).

31 Lespade, P., Marchand, A., Couzi, M. & Cruege, F. Caracterisation de materiaux carbones par microspectrometrie Raman. *Carbon* **22**, 375-385, (1984).

32 Ping. J. *et al.* Layer Number and Stacking Sequence Imaging of Few-Layer Graphene by Transmission Electron Microscopy. *Nano Lett.* **12**, 4635-4641, (2012).

33 Brown. L. *et al.* Twining and Twisting of Tri- and Bilayer Graphene. *Nano Lett.* **12**, 1609-1615, (2012).

34 Shevitski. B. *et al.* Dark-Field Transmission Electron Microscopy and the Debye-Waller Factor of Graphene. *Phys. Rev. B* **87**, 045417, (2013).

35 Ōya, A. & Marsh, H. Phenomena of catalytic graphitization. *J. Mater. Sci.* **17**, 309-322, (1982).

36 Feates, F. S. The diffusion of carbon in single crystal graphite. *J. Nucl. Mater.* **27**, 325-330, (1968).

37 Thrower, P. A. & Mayer, R. M. Point defects and self-diffusion in graphite. *Phys. status solidi (a)* **47**, 11-37, (1978).

38 Cunning, B. C., Wang, B., Ruoff, R. S. Structure-Directing Effect of Single Crystal Graphene Film on Polymer Carbonization and Graphitization. *Mater. Horiz.* **6**, 796-801, (2019).

39 Oberlin, A. Carbonization and Graphitization. *Carbon* **22**, 521-541, (1984).

40 Mason, I. B. & Knibbs, R. H. The Young's modulus of carbon and graphite artefacts. *Carbon* **5**, 493-506, (1967).

41 Kazuyuki, I., Masayuki, K., Tadashi, S. & Yuji, A. Electrical Resistivity Measurements of Layer Number Determined Multilayer Graphene Wiring for Future Large Scale Integrated Circuit Interconnects. *Japan. J. Appl. Phys.* **52**, 06GD08 (2013).

42 Moore, A.W. Chemistry and Physics of Carbon. 69, (Vol. 11, Walker, Jr. P. L., Thrower, P. A. (Eds.) Marcel Dekker, NewYork, 1973).

43 Deprez, N. & McLachlan, D. S. The Analysis of the Electrical Conductivity of Graphite Conductivity of Graphite Powders during Compaction. *J. Phys. D: Appl. Phys.* **21**, 101-107, (1988).

44 Rani, A., Nam, S., Oh, K. A. & Park, M. Electrical Conductivity of Chemically Reduced Graphene Powders under Compression. *Carbon Lett.* **11**, 90-95, (2010).

45 Ghosh, W. *et al.* Dimensional Crossover of Thermal Transport in Few-Layer Graphene, *Nat. Mater.* **9**, 555–558, (2010).

46 Wang, L., Metcalf, S., Critoph, R., Thorpe, R., Tamainot-Telto, Z. Thermal Conductivity and Permeability of Consolidated Expanded Natural Graphite Treated with Sulphuric Acid. *Carbon* **49**, 4812-4819 (2011).

47 A. I. S. Panasonic Corporation, Company. (2017. (https://industrial.panasonic.com/cdbs/www-data/pdf/AYA0000/AYA0000C27.pdf)).

48 Peng, L. *et al.*, Ultrahigh Thermal Conductive yet Superflexible GrapheneFilms. *Adv. Mater.* **29**, 1700589 (2017).

49 Hu, D. *et al.*, Strong Graphene-Interlayered Carbon Nanotube Films with High Thermal Conductivity. *Carbon* **118**, 659-665 (2017).

50 Ding, J. *et al.*, Hydroxylated Graphene-Based Flexible Carbon Film with Ultrahigh Electrical and Thermal Conductivity. *Nanotechnology* **28**, 39LT01 (2017).

Acknowledgments:

We appreciate comments by Peter Thrower, Revathi Bacsa, and Leonard Interrante. This work was supported by the Institute for Basic Science (IBS-R019-D1). ZL and HS acknowledge financial support from the National Natural Science Foundation of China (No.51402291). A.A.B. and F.K. acknowledge support from the Spins and Heat in Nanoscale Electronic Systems (SHINES) Center funded by the U.S. Department of Energy under Award # SC0012670.

Author contributions: R.S.R. supervised the project. B.W., B.V.C., and R.S.R. conceived the experiments. B.W., V.M., and Y. S. prepared the stacked graphene samples. B.W., B.V.C., L.P., C.G., and X.C. contributed to the heat treatment of the samples. W.K.S., B.V.C., V.M.,

and Y.K. put efforts into the heating systems design. T.J.S. helped with the synchrotron GIWAXS measurement and analysis. N.Y.K. and Z.L. performed TEM analysis. S.Y.P. and J.Y.K. contributed to the mechanical measurement and analysis. J.J. and K.K. measured the resistance of the materials. F.K. and A.A.B. analyzed the thermal conductivity data with assistance from S.R.K and G-H. K. Z.L. and H.S. provided the monolayer graphene film samples. B.W., B.V.C., and R.S.R. wrote the manuscript. All co-authors revised and commented on the manuscript.

Competing interests: Authors declare no competing interests.

Data and materials availability: All data is available in the main text or the Supporting Information.

Supporting Information:

Methods

Figures S1-S27

Tables S1-S6

References (*S1-S12*)

Stacked CVD graphene when heat-treated results in a macro-scale graphitic film with mixed AB/incommensurate stacking through each layer but near perfect in-plane order. This graphitic film has mechanical performance greatly exceeding all macro-scale layered graphitic films, and an exceptionally high in-plane thermal conductivity.

Keyword Graphene

Bin Wang, Benjamin V. Cunning,* Na Yeon Kim, Fariborz Karger, Sun-Young Park, Zhancheng Li, Shalik R. Joshi, Li Peng, Vijayakumar Modepalli, Xianjue Chen, Yongtao Shen, Won Kyung Seong, Youngwoo Kwon, Jeongsu Jang, Haofei Shi, Chao Gao, Gun-Ho Kim, Tae Joo Shin, Kwanpyo Kim, Ju-Young Kim, Alexander A. Balandin, Zonghoon Lee, Rodney S. Ruoff*

Title Ultra-stiff, strong, and highly thermally conductive crystalline graphitic films with mixed stacking order